Inorganic Fullerenes

DOI: 10.1002/anie.201006719

MoS_2 Hybrid Nanostructures: From Octahedral to Quasi-Spherical Shells within Individual Nanoparticles**

Ana Albu-Yaron, Moshe Levy, Reshef Tenne, Ronit Popovitz-Biro, Marc Weidenbach, Maya Bar-Sadan, Lothar Houben, Andrey N. Enyashin, Gotthard Seifert, Daniel Feuermann, Eugene A. Katz, and Jeffrey M. Gordon**

MoS_2, a layered compound with tribological and catalytic applications, is known to form a range of hollow closed nanostructures[1–5] and nanoparticles, including graphene-like structures.[6] These have been demonstrated experimentally through high-temperature synthesis and pulsed laser ablation (PLA), and theoretically with quantum chemical calculations. The smallest allowed structures are nanooctahedra of 3 to 8 nm size. Nicknamed the "true inorganic fullerene" in analogy to carbon fullerenes,[4] they differ from larger multi-walled MoS_2 fullerene-like nanoparticles both in their morphology and predicted electronic properties. The larger fullerene-like particles are quasi-spherical (polyhedral) or nanotubular, typically with diameters of 20 to 150 nm.[3] Above a few hundred nm in size, these nanoparticles transform into 2H-MoS_2 platelets. Fullerene-like particles have been recognized as superior solid lubricants[7] with numerous commercial applications, and MoS_2 nanooctahedra may have catalytic applications. Understanding the fundamental commonality of these two morphologies might prove essential in the development of new materials.

[*] Dr. A. Albu-Yaron, Prof. Dr. M. Levy, Prof. Dr. R. Tenne
Department of Materials and Interfaces
Weizmann Institute of Science, Rehovot 76100 (Israel)
E-mail: reshef.tenne@weizmann.ac.il
Prof. Dr. D. Feuermann, Dr. E. A. Katz, Prof. Dr. J. M. Gordon
Department of Solar Energy and Environmental Physics, Jacob Blaustein Institutes for Desert Research, Ben-Gurion University of the Negev, Sede Boqer Campus 84990 (Israel)
E-mail: jeff@bgu.ac.il
Dr. R. Popovitz-Biro
Electron Microscopy Unit
Weizmann Institute of Science, Rehovot 76100 (Israel)
M. Weidenbach, Dr. M. Bar-Sadan, Dr. L. Houben
Institute of Solid State Research and Ernst Ruska Centre for Microscopy and Spectroscopy with Electrons, Forschungszentrum Jülich GmbH (Germany)
Dr. A. N. Enyashin, Prof. Dr. G. Seifert
Physikalische Chemie, Technische Universität Dresden (Germany)

[**] R.T. gratefully acknowledges the support of ERC project INTIF 226639, the Israel Science Foundation, the Harold Perlman Foundation, and the Irving and Cherna Moskowitz Center for Nano and Bio-Nano Imaging. R.T. is the Drake Family Chair of Nanotechnology and director of the Helen and Martin Kimmel Center for Nanoscale Science.

The research on hollow MoS_2 nanostructures of minimal size (< 10 nm in diameter) was initiated in 1993 upon the first independent proposal of the formation of nanooctahedra of MoS_2[3,5] (and BN)[8] with six rhombi in their corners. In 1999, it was demonstrated[4] that two- to four-walled MoS_2 nanooctahedra, 3–5 nm in size and up to ca. 10^4 atoms, could be obtained by PLA. Similar results were subsequently reported in Ref. [1,2] as illustrated in Figure 1 a. Recent studies of high energy density methods such as laser ablation and arc–discharge[9–13] resulted in small structures with only a limited number of atoms: Mo–S clusters or double-walled nanooctahedra.

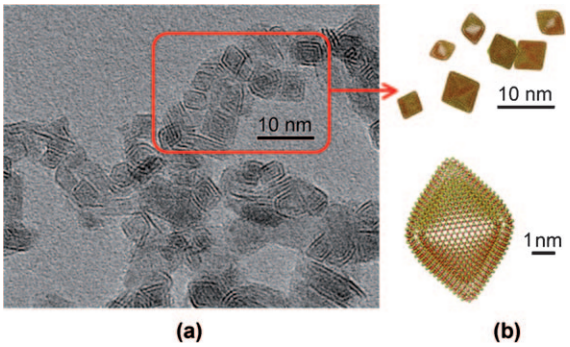

Figure 1. a) Transmission electron microscope (TEM) image that includes MoS_2 nanooctahedra generated from MoS_2 powder by PLA as reported in Ref. [1,2]. Note the large number of nanooctahedra with two or three layers and < 8 nm in size. b) Ball-and-stick models showing assorted projections of the nanooctahedra in (a), where Mo atoms are red and S atoms are yellow.

On the other hand, theoretical modeling[1,2] suggested that the stability limit for nanooctahedra should be almost an order of magnitude larger than the largest structures produced by PLA (see Figure 3 of Ref. [1]). Therefore, nanooctahedra with more than five layers were not considered in modeling procedures. A principal insight from the PLA studies was that the low density of the Mo–S vapor, coupled with the rapid temperature quench, prevented the nanooctahedra from growing to sizes large enough to realize their stability limit. It was concluded that a two-step process of PLA at 2000 °C, followed by in situ annealing at 500–750 °C, is advantageous for improving the yield of MoS_2 nanooctahedra.[1,2,14] In contrast, substantial amounts of larger multi-walled quasi-spherical or nanotubular structures were pro-

duced by oven-driven reactions, but without nanooctahedra. Most likely the internal energy of the process was insufficient for the required transformation,[15–20] the nature of which has not been elucidated to date.

The confluence of these results, and the success of purely photothermal PLA, prompted the development of alternative optical systems (such as solar and discharge lamp concentrators),[21] and culminated in the development of a high-irradiance solar furnace[22] shown in Figure 2. This experimental facility provides high power densities (ca. 15000 suns, i.e., 15 W mm^{-2}) on sizable areas (of the order of several mm^2)

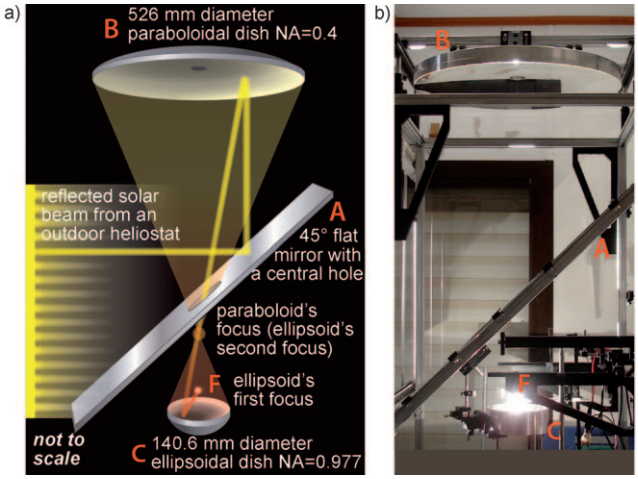

Figure 2. High-irradiance solar furnace. a) Schematic. b) Side photograph. Ambient sunlight is reflected into the laboratory from an outdoor flat dual-axis tracking mirror, and redirected by a flat 45° mirror (**A**) to a downward-facing specular paraboloidal dish (**B**) with its focus just below the tilted mirror. Flux concentration is boosted to ca. 15000 suns by a specular ellipsoidal dish (**C**) of high numerical aperture NA at its proximate focus **F** (attainable flux density is proportional to NA^2). The quartz ampoule was inserted to **F** horizontally from the right, and translated horizontally by 1 mm each minute toward irradiating as much of the distributed precursor powder as possible.

in a continuous fashion. Relative to PLA systems, the solar furnace provides a larger reaction volume and higher vapor pressure of reactants, with peak reactor temperatures >2700 K.[23] Thermal radiation from the heated precursor powder provides a natural, extensive, and hot annealing environment.

Figure 3 shows representative nanoparticles obtained by ablating MoS_2 powder in a sealed, evacuated quartz ampoule in the above mentioned solar furnace. These MoS_2 nanostructures likely start growing from the inside out (Figure 3a–e). This growth mode is typical for a nucleation and growth mechanism from the vapor phase,[24] and differs markedly from the outside–in growth mode where molybdenum oxide nanoparticles serve as a template for the reaction with H_2S.[18] When the nanooctahedra exceed a critical size, the layers should start to fold evenly and transform into quasi-spherical shape. The TEM images reveal multi-walled nanooctahedra at the core up to a diameter slightly above 10 nm or ca. 10^5 atoms beyond which the elastic strain is better accommodated by adopting an even folding of the layers into quasi-spherical shells. Tilted structures (Figure 3c,d) reveal the inner core morphology, which is similar to that reported earlier for the smaller nanooctahedra.[1,4] The size of the hybrid nanoparticles' hollow core is determined by the maximum strain the MoS_2 nanooctahedra can accommodate, i.e., their minimum size, which is ca. 3 nm.[1,4]

A detailed phenomenological model that incorporates semi-empirical density functional methods[1,2] and has been shown to account for experimentally observed MoS_2 nanostructures ranging from fundamentally small (ca. 3 nm) to large closed-cage fullerene-like and nanotubular configurations (diameters up to 100 nm) was adopted for gaining insight into, and predicting, nanostructure stability and electronic properties. The predicted electronic properties, derived from the structural features, showed that the lattice defects associated with the formation of the nanooctahedra may induce a metallic-like nature, while quasi-spherical structures are semiconducting.

This model was used here to assess the relative stability of hollow hybrid MoS_2 nanoparticles comprising octahedral (subscript o) and spherical (subscript s) shells by estimating the energy relative to the monolayer ΔE. For each individual shell i of diameter D_i, where N denotes the number of atoms in a given shell, a is the lattice parameter for a MoS_2 monolayer (0.316 nm),[25] β is the elasticity factor (1370 eV),[2] and $\Delta\varepsilon_r$ and $\Delta\varepsilon_p$ are the energies of the atoms at the edges and corners of the nanooctahedra (1.45 and 3.72 eV per atom, respectively).[25]

$$\Delta E_s = \frac{\sqrt{3}a^2\beta}{6\pi D_s^2};\ N_s = \frac{6\pi D_s^2}{\sqrt{3}a^2} \tag{1}$$

$$\Delta E_o = \frac{3\Delta\varepsilon_r\left(\sqrt{2}aD_o^2 - 6a^2\right) + 18a^2\Delta\varepsilon_p}{D_o^2};\ N_o = \frac{2D_o^2}{a^2} \tag{2}$$

The energy of the full hollow hybrid nanostructure comprising o nested nanooctahedra inserted into s spherical shells is

$$\Delta E = \frac{\sum_s \Delta E_s + \sum_o \Delta E_o}{\sum_s N_s + \sum_o N_o} + \frac{k-1}{k}\varepsilon_{\mathrm{vdW}},\ o+s=k,\ D_{i+1} - D_i = \frac{c}{2} \tag{3}$$

where c is the lattice parameter for bulk 2H-MoS_2 (1.23 nm),[26] and $\varepsilon_{\mathrm{vdW}}$ is the van der Waals energy of interlayer interaction (-0.2 eV per atom).[25] A simplifying assumption was that the outer MoS_2 walls are perfectly spherical, which neglects the contribution of the cusps where the folding is uneven. This simplification is deemed accurate enough for this investigation, given the agreement between model predictions and experimental observations (see below).

The predictions plotted in Figure 4 confirm that the model can indeed account for the coexistence of nested MoS_2 octahedra and peripheral spherical shells, with a smooth transition from nanoclusters dominated by octahedra to those dominated by spherical shells as the particle size and number of layers increase. For a fixed total number of layers (taken to be 10, 20, and 30) and nanoparticle diameter (ranging from 13

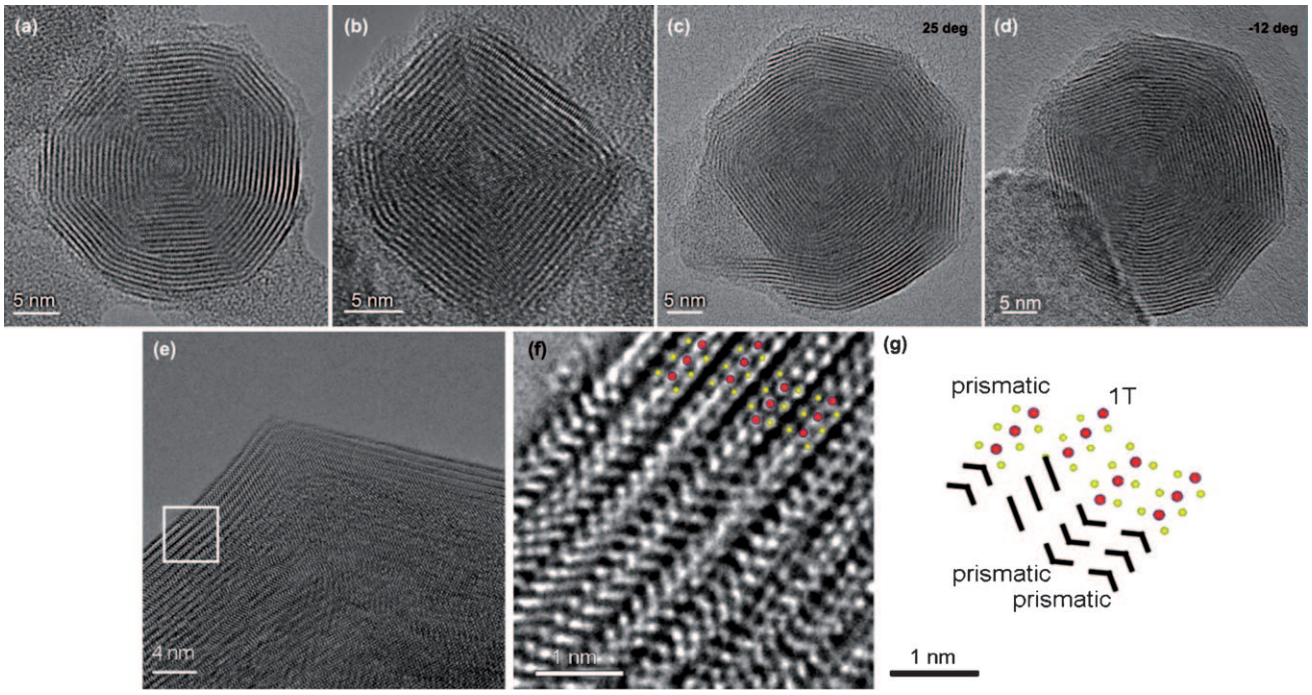

Figure 3. Typical MoS_2 closed nanoparticles in which a nanooctahedral core undergoes morphology change to quasi-spherical outer shells, obtained in the solar furnace. a,b) Two hybrid nanoclusters of roughly the same diameter (ca. 26 nm) and number of layers (ca. 20). c,d) TEM tilting experiment of an individual hybrid MoS_2 nanoparticle of diameter 43 nm and 28 layers, substantially larger than those in (a) and (b), and reinforcing the clarity of the transition from core octahedra to surrounding quasi-spherical shells. e) High-resolution TEM images of a hybrid nanoparticle. The marked frame is enlarged in (f), showing atomic resolution of the MoS_2 layers. The atomic model is overlaid in red (Mo) and yellow (S), and detailed in (g) with black lines as visual guides to their appearance in the TEM image. The chevron motif correlates with a prismatic coordinated MoS_2 layer, which as a bulk phase is semiconducting. The pattern of diagonal lines indicates the 1T phase, which has been predicted to be metallic.[25]

to 60 nm), there is a thermodynamically preferred mix of octahedral and spherical shells, i.e., a minimum in the curves of Figure 4, all of which are more stable than the monolayer. The existence and sharpness of these minima become less pronounced, and the nanoparticles become dominated by spherical layers, as the nanostructures grow larger. For example, if a MoS_2 nanoparticle reaches a diameter of at least 44 nm, then its most stable composition becomes solely spherical shells. Note that the 44 nm curves for nanoparticles with a total of 10, 20, and 30 layers exhibit a broad range of essentially equal-stability hybrid compositions rather than an evident minimum.

The consistency of model predictions with experimental findings is highlighted in Figure 4 with indicators for the nanostructures of both Figure 3a (26 nm in diameter and ca. 20 shells of which 10 are spherical) and Figure 3c,d (44 nm in diameter and 30 shells of which 20 are spherical). The indistinctness in deciphering the fraction of octahedral layers in the nanostructures of Figure 3 is reflected in the broad theoretical minima of Figure 4.

Another consideration is that the model is purely thermodynamic, disregarding kinetic effects that may not be insubstantial for rapidly evolving structures, and could result in hollow hybrid nanostructures other than those of the local minima in Figure 4[27]—especially given the non-equilibrium reactor conditions. This may also play a role in explaining the production of nanoparticles such as in Figure 3b, where, for approximately the same size and total number of layers as in Figure 3a, the octahedral core layers dominate to a noticeably greater degree.

Band-structure calculations[2] indicate that the corners and edges of the pure nanooctahedra induce states within the Fermi level, rendering a metallic character to a pure nanooctahedral shell. In contrast, both theory[28,29] and experiment[30,31] have shown that, in analogy to the bulk material, larger fullerene-like and nanotubular MoS_2 nanostructures are semiconductors irrespective of their chirality vector. Consequently, the transition from inner nanooctahedra to quasi-spherical outer shells may mark a transition from metallic-like layers to semiconducting ones.

A second structural feature to be considered is that MoS_2 has multiple bulk phases which exhibit different electronic properties. MoS_2 layers form two trigonal prismatic bulk phases: 2H (anti-parallel) and 3R (parallel), the former being more stable. Both phases are semiconducting.[32] An octahedrally coordinated phase (1T) also exists and was predicted to be metallic,[25] but is not stable in the bulk form, and is associated solely with MoS_2 monolayers. Both the 2H and 3R phases have been observed in closed-cage structures; but so far not the 1T phase. Therefore, the internal structure of the particle may also have a distinct influence on the electronic properties of the hybrid particle.

The X-ray diffraction measurements are strongly affected by disorder and strain, which encumbers the delicate differ-

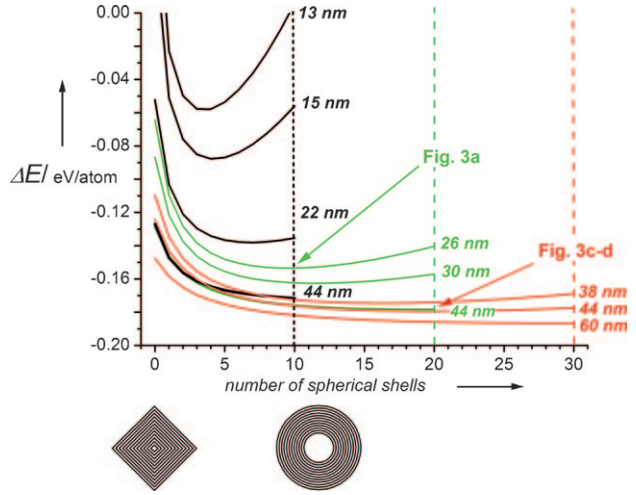

Figure 4. Energy (relative to that of a monolayer) of hollow hybrid MoS_2 nanostructures comprising nested nanooctahedra inside spherical shells, as a function of the number of spherical shells, for a range of values of the 1) total number of layers (10 (black), 20 (green), and 30 (red)), and 2) outer diameter (nm label to the right of each curve). The schematics below the graph illustrate the extremes of pure octahedral and pure spherical structures (in this instance for 12 layers). The properties of the experimentally generated nanoparticles of Figure 3 are indicated by arrows. The nanostructure of Figure 3a is close to the model's energetic minimum for a total of ca. 20 layers of which ca. 10 are spherical, and a diameter of 26 nm, for which the model indicates 720000 atoms, i.e., 240000 stoichiometric MoS_2 units. The nanostructure of Figure 3c,d, with a diameter of 44 nm and ca. 20 spherical shells, is consistent with the model's broad range of equally low-energy configurations for a total of 30 layers and the same diameter.

entiation between the 2H and 3R phases. Hence the focus here was on straightforward direct imaging. The diffraction data comprise a basis for future research that will take into account strain effects within these closed-cage structures, and will be complemented by electron diffraction data.

The question of atomic-scale coordination prompted examining the hybrid nanostructures by aberration-corrected TEM[33] (Figure 3f). The aberration-corrected TEM revealed first-ever 1T coordination of layers embedded within nanoparticles (Figure 3e–g), with Figure 3f clearly showing the different MoS_2 layers. Figures 3f,g reveal a single 1T layer between prismatic layers: to its right is an anti-parallel alignment of the prismatic layers, and to its left a single prismatic layer. The scarcity of the 1T phase in previously reported structures may be related either to the number of layers lying below the detection limit of XRD or Raman measurements, or to the relative instability of the 1T phase, which prevents the formation of multiple 1T shells. The occurrence of the 1T phase may be the result of a transformation from the 3R to the 2H phase by an intermediate 1T phase that is trapped by fast quenching. Nevertheless, the incorporation of a single 1T layer might have substantial effects on the electronic properties of the whole particle, since the phase multiplicity may induce inner metal–semiconductor junctions. The two structural features contributing to the formation of such "buried" junctions in a spherical geometry raise new, fundamental questions regarding their electronic properties. These features are the focus of ongoing experimental and theoretical research.

The discovery of these hybrid particles bridges the gap between the two limits of pure, fundamentally small nanooctahedra and markedly larger quasi-spherical nanoparticles. The two nanostructures coexist within an individual nanoparticle, with a near-seamless transition from a core of octahedral layers to a peripheral region of quasi-spherical shells. Such nanostructures, if produced in large amounts, could reveal new electrical, optical, and possibly catalytic characteristics. Other applications, including the well-established one for solid lubrication, remain to be investigated when larger amounts of such nanoparticles can be synthesized.

The solar concentrator optics depicted here created reactor conditions of continuous ultra-high irradiance, high temperature, large reaction volumes, and extended hot annealing conditions that produced an unpredicted, fundamental, and previously unobserved family of hybrid MoS_2 nanostructures. An extended phenomenological model was used to calculate their critical sizes, the number of MoS_2 layers, and the mix of octahedral and quasi-spherical layers for this transition, and found to agree with the experimental observations. The hybrid nanoparticles are 25 to 45 nm in diameter, with the fraction of the layers comprising the inner octahedra decreasing as the nanoparticles grow larger. Kinetically controlled nanostructures dominated by the octahedral core layers were also observed. In addition, atomic-scale features identified by aberration-corrected high-resolution TEM suggest that the hybrid particle has a complex unprecedented electronic structure.

To summarize, a fundamentally new MoS_2 fullerene-like nanostructure was realized exhibiting a smooth transition from a nanooctahedral core to quasi-spherical outer shells within individual nanoparticles, with corroborating theoretical modeling and atomic resolution transmission electron microscopy. The transformations are driven by an ultra-high irradiance solar concentrator that produces the requisite high temperatures, large reaction volumes, and naturally hot annealing environments. Unraveling the internal structure of these hybrid nanoparticles suggests the existence of metal–semiconductor junctions within individual nanoparticles.

Received: October 26, 2010
Published online: January 14, 2011

Keywords: hybrid compounds · inorganic fullerenes · molybdenum sulfide · nanoparticles · solar ablation

[1] A. N. Enyashin, S. Gemming, M. Bar-Sadan, R. Popovitz-Biro, S. Y. Hong, Y. Prior, R. Tenne, G. Seifert, *Angew. Chem.* **2007**, *119*, 631–635; *Angew. Chem. Int. Ed.* **2007**, *46*, 623–627.
[2] M. Bar-Sadan, A. N. Enyashin, S. Gemming, R. Popovitz-Biro, S. Y. Hong, Y. Prior, R. Tenne, G. Seifert, *J. Phys. Chem. B* **2006**, *110*, 25399–25410.
[3] L. Margulis, G. Salitra, M. Talianker, R. Tenne, *Nature* **1993**, *365*, 113–114.
[4] P. A. Parilla, A. C. Dillon, K. M. Jones, G. Riker, D. L. Schulz, D. S. Ginley, M. J. Heben, *Nature* **1999**, *397*, 114.

[5] R. Tenne, *Adv. Mater.* **1995**, *7*, 965 – 995.
[6] H. S. S. Ramakrishna Matte, A. Gomathi, A. K. Manna, D. J. Late, R. Datta, S. K. Pati, C. N. R. Rao, *Angew. Chem.* **2010**, *122*, 4153 – 4156; *Angew. Chem. Int. Ed.* **2010**, *49*, 4059 – 4062.
[7] L. Rapoport, Y. Bilik, Y. Feldman, M. Homyonfer, S. R. Cohen, R. Tenne, *Nature* **1997**, *387*, 791 – 793.
[8] F. Jensen, H. Toftlund, *Chem. Phys. Lett.* **1993**, *201*, 89 – 96.
[9] D. M. D. J. Singh, T. Pradeep, J. Bhattacharjee, U. V. Waghmare, *J. Phys. Chem. A* **2005**, *109*, 7339 – 7342.
[10] R. Sen, A. Govindaraj, K. Suenaga, S. Suzuki, H. Kataura, S. Iijima, Y. Achiba, *Chem. Phys. Lett.* **2001**, *340*, 242 – 248.
[11] S. Gemming, G. Seifert, M. Götz, T. Fischer, G. Ganteför, *Phys. Status Solidi B* **2010**, *247*, 1069 – 1076.
[12] L. Chang, H. Yang, J. Li, W. Fu, Y. Du, K. Du, Q. Yu, J. Xu, M. Li, *Nanotechnology* **2006**, *17*, 3827 – 3831.
[13] I. Alexandrou, N. Sano, A. Burrows, R. R. Meyer, H. Wang, A. I. Kirkland, C. J. Kiely, G. A. J. Amaratunga, *Nanotechnology* **2003**, *14*, 913 – 917.
[14] A. N. Enyashin, M. Bar-Sadan, J. Sloan, L. Houben, G. Seifert, *Chem. Mater.* **2009**, *21*, 5627 – 5636.
[15] M. Remskar, *Adv. Mater.* **2004**, *16*, 1497 – 1505.
[16] W. K. Hsu, B. H. Chang, Y. Q. Zhu, W. Q. Han, H. Terrones, M. Terrones, N. Grobert, A. K. Cheetham, H. W. Kroto, D. R. M. Walton, *J. Am. Chem. Soc.* **2000**, *122*, 10155 – 10158.
[17] J. Chen, N. Kuriyama, H. Yuan, H. T. Takeshita, T. Sakai, *J. Am. Chem. Soc.* **2001**, *123*, 11813 – 11814.
[18] R. Rosentsveig, A. Margolin, A. Gorodnev, R. Popovitz-Biro, Y. Feldman, L. Rapoport, Y. Novema, G. Naveh, R. Tenne, *J. Mater. Chem.* **2009**, *19*, 4368 – 4374.
[19] F. L. Deepak, A. Mayoral, M. J. Yacaman, *Appl. Phys. A* **2009**, *96*, 861 – 867.
[20] J. Etzkorn, H. A. Therese, F. Rocker, N. Zink, U. Kolb, W. Tremel, *Adv. Mater.* **2005**, *17*, 2372 – 2375.
[21] I. Wiesel, H. Arbel, A. Albu-Yaron, R. Popovitz-Biro, J. M. Gordon, D. Feuermann, R. Tenne, *Nano Res.* **2009**, *2*, 416 – 424.
[22] J. M. Gordon, D. Babai, D. Feuermann, *Sol. Energy Mater. Sol. Cells* **2011**, *50*, DOI: 10.1016/j.solmat.2010.11.030.
[23] M. Levy, A. Albu-Yaron, R. Tenne, D. Feuermann, E. A. Katz, D. Babai, J. M. Gordon, *Isr. J. Chem.* **2010**, *50*, 417 – 425.
[24] A. Margolin, R. Popovitz-Biro, A. Albu-Yaron, A. Moshkovich, L. Rapoport, R. Tenne, *Chem. Phys. Lett.* **2005**, *411*, 162 – 166.
[25] F. Wypych, R. Schöllhorn, *J. Chem. Soc. Chem. Commun.* **1992**, 1386 – 1388.
[26] T. Böker, R. Severin, A. Müller, C. Janowitz, R. Manzke, D. Voß, P. Krüger, A. Mazur, J. Pollmann, *Phys. Rev. B* **2001**, *64*, 235305.
[27] D. J. Srolovitz, S. A. Safran, M. Homyonfer, R. Tenne, *Phys. Rev. Lett.* **1995**, *74*, 1779 – 1782.
[28] G. Seifert, T. Köhler, R. Tenne, *J. Phys. Chem. B* **2002**, *106*, 2497 – 2501.
[29] G. Seifert, H. Terrones, M. Terrones, G. Jungnickel, T. Frauenheim, *Phys. Rev. Lett.* **2000**, *85*, 146 – 149.
[30] G. L. Frey, S. Elani, M. Homyonfer, Y. Feldman, R. Tenne, *Phys. Rev. B* **1998**, *57*, 6666 – 6671.
[31] I. Milosevic, B. Nikolic, E. Dobardzic, M. Damnjanovic, I. Popov, G. Seifert, *Phys. Rev. B* **2007**, *76*, 233414.
[32] J. A. Wilson, A. D. Yoffe, *Adv. Phys.* **1969**, *18*, 193 – 335.
[33] M. Bar-Sadan, L. Houben, A. N. Enyashin, G. Seifert, R. Tenne, *Proc. Natl. Acad. Sci. USA* **2008**, *105*, 15643 – 15648.

